SCIENTIFIC CULTURE
www.sci-cult.com

SCIENTIFIC CULTURE, Vol. 12, No. 5, (2026), pp. 446-461
Open Access. Online & Print

DOI: 10.5281/zenodo.1250040

ADDITIVE MANUFACTURING FOR GAS TURBINE BURNER REPAIR: A CASE STUDY

Dr Aiyad Gannan[1], Dr Nader Ghareeb[2], Dr. Wisam Al Saadi[3]

[1] *Assistant Professor, Mechanical Eng Technology, University of Doha for Science and Technology, Qatar*
[2] *Assistant Professor, Mechanical Engineering, Australian University of Kuwait, Kuwait*
[3] *Associate Professor, Mechanical Engineering, Department of Mechanical Engineering, College of Engineering, Australian University Kuwait*

Received: 11/12/2025
Accepted: 25/02/2026

Corresponding author: Dr Aiyad Gannan
(aiyad.gannan@udst.edu.qa)

ABSTRACT

Additive manufacturing (AM) is gaining more popularity in the industry. It involves adding material to create new objects or repairing existing damaged ones. This approach avoids issues like warping and internal stress in machining. Rapid prototyping, a form of AM, offers benefits such as lower manufacturing costs, reduced production time, improved accuracy, and higher quality. AM is particularly useful for creating complex geometrical designs that are challenging or impossible with traditional methods. This work outlines the fundamental characteristics of additive manufacturing techniques applied to repairing and improving a Gas Turbine (GT) burner. Two distinct repair scenarios of the damaged burner are proposed and implemented through simulation by using the finite element method. The damaged burner face is machined in the first scenario, and Hastelloy X is printed on top of the stainless-steel body. The second scenario takes it further by machining the damaged burner face, printing Hastelloy X, and imposing additional cooling measures. Scenarios have presented effective solutions for repairing the damaged surface. However, after careful evaluation, it has been concluded that the second scenario has the potential for future development as it extends the life cycle of the GT burner from 16k to 32k-48k hours. A feasibility study was also conducted to demonstrate that repairing a damaged pilot burner is financially less expensive compared to purchasing a new burner. Thus, the savings could reach about $1.22 million to repair a total of 450 burners, assuming each burner has a service life of 48,000 operating hours.

KEYWORDS: Additive manufacturing (AM), Rapid prototyping, GasTurbine, Burner, Repair, Simulation

Copyright: © 2026. This is an open-access article distributed under the terms of the Creative Commons Attribution License. (https://cre-ativecommons.org/licenses/by/4.0/).

1. INTRODUCTION

Additive manufacturing (AM), also known as 3D printing, is a rapidly growing revolutionary manufacturing process which enables the creation of complex three-dimensional objects with un-precedented precision and efficiency [1-4]. Unlike traditional subtractive manufacturing methods, AM involves a set of computer-automated processes that lead to building physical objects layer by layer using digital design data, including computer-aided design (CAD) models (See Fig. 1). These physical objects are fabricated using various plastic, ceramic, metallic, biological, or even composite materials and polymers [5, 6] in a fast production rate and with less cost and material wastage [7, 8]. AM has further developed and blossomed into an abundance of processes, including laser metal deposition (LMD), stereolithography (SLA), binder jetting, direct metal deposition (DMD), selective laser sintering (SLS), laminated object manufacturing (LOM), fused deposition modeling (FDM), inkjet printing, selective laser melting (SLM) and others [9, 10]. AM has plenty of applications across various engineering fields including Aerospace and automotive fields [11-14], medical field [15, 16], architecture [17], fashion [18], and even food industry [19]. Furthermore, the integration of Artificial Intelligence (AI) in AM operations contributed among others to increasing the prefabrication efficiency, thus resulting in a more reliable and cost-effective production [20-22].

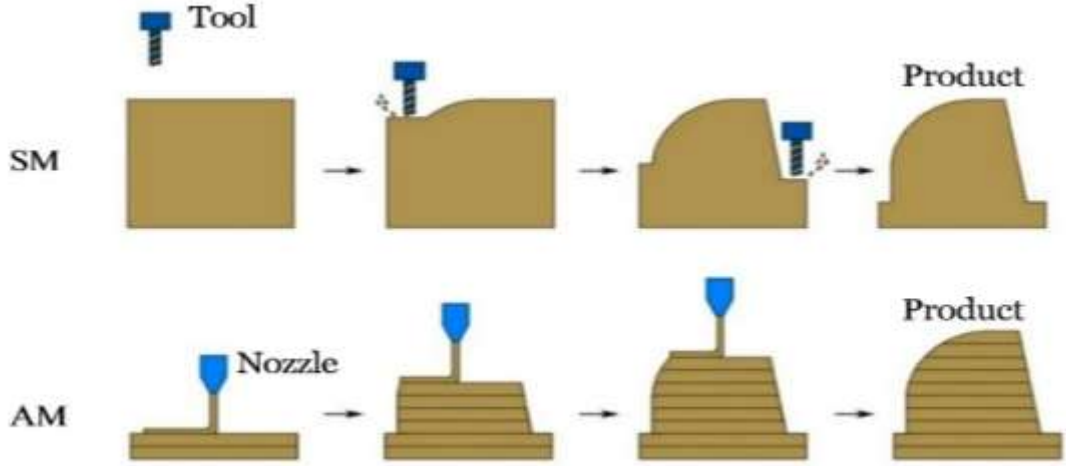

Figure 1: A comparison between subtractive manufacturing and additive manufacturing [11].

In addition to what has been mentioned, AM has a high potential to improve the repair and performance of mechanical parts, including gas turbines. However, only a few studies were conducted in this regard. Arjakine et al. discussed the advanced welding processes that Siemens Power Generation uses to repair gas turbine hot-section components, focusing mainly on the blades [21]. Charles and Taylor demonstrated how the electron beam melting AM is implemented to develop a frame- work for repairing the gas turbine blades and rubbing marks on stationary vanes or guide rings [23]. Wilson et. al. presented the successful repair of defective voids in turbine airfoils using the laser direct deposition AM technology [24]. Polyanskii et. al. proposed the abrasive jet machining AM technique for performing repair operations on gas turbines' rotor and blades [25]. Schurb et. al. explored the effectiveness and the validity of the gas turbine parts produced using the Direct Metal Laser Melting (DMLM) AM technology [26]. Gebisa and Lemu investigated the existing metal AM techniques and materials regarding their applicability to producing gas turbine engine components [1]. It can be noted that all the previously presented papers focused on repairing the gas turbine blades only. To the best of the authors' knowledge, there is no sufficient information on how to repair other components of the gas turbine, especially the gas turbine burner, using the AM technology. The only available research on this topic investigates the application of laser metal deposition (LMD) as a repair technique for gas turbine burners, and it is limited to burners made of Inconel 718 only, where only the experimental results of repairing Inconel 718 gas turbine burners using LMD were presented [27].

In contrast to previous studies that primarily focused on gas turbine blades, this work specifically investigates the repair and life extension of gas turbine pilot burners using additive manufacturing techniques. To the best of the authors' knowledge, a systematic thermo-mechanihave evaluation of burner repair through Laser Beam Powder Bed Fusion (LB-PBF) combined with reverse engineering and enhanced cooling strategies has not been comprehensively reported in the literature. The

novelty of this study lies in (i) the integration of material replacement with Hastelloy X using LB-PBF, (ii) the comparative assessment of two repair configurations through coupled thermo-mechanical finite element analysis, and (iii) the incorporation of additional cooling channels to significantly extend service life. Unlike conventional repair approaches, the proposed methodology combines structural redesign and thermal management to achieve a life extension from 16,000 hours to 32,000–48,000 hours while maintaining economic feasibility. This integrated engineering approach provides a practical and scalable repair strategy for industrial gas turbine burners and contributes to bridging the existing research gap in additive manufacturing-based burner refurbishment.

2. PROBLEM DEFINITION AND METHODOLOGY

Most GT failures occur in the hot section, where components like combustor liners, transition pieces, vanes, and blades operate in a harsh environment with high temperatures and stresses [28]. Analyzing hot section failures requires a combined metallurgical-mechanical engineering approach to get the most information out of each failure event. However, these incidents can be utilized effectively to enhance the equipment's design, operation, and maintenance practices. Direct observations during 8k and 16k inspections for gas turbine engines indicated that multiple cracks exist. These cracks extend from the centre face toward the igniter and liquid holes of the burners, as shown in Fig. 2. The crack initiation, propagation, and fatigue fracture could result from high thermal stresses and thermal cyclic fatigue [29, 30].

Figure 2: Gas turbine pilot burner crack.

Thermal fatigue is specified as the main reason for the crack creation in gas turbine components [31]. Its life in gas turbine burners is directly related to stress and strains due to the thermal gradients generated by combustion gas flow and the circulating air. Tensile stresses, induced by low temperatures, are a critical and damaging factor concerning fatigue failures [32, 33]. Furthermore, the variation in the gas turbine pilot burner temperature from the center face to the edge is from 990◦C to 350◦C, which is significantly high. Moreover, the start/stop of the gas turbine can also create a rapid rate of change in temperature fluctuation, thereby inducing thermal stresses and initiating the occurrence of material cracking, which will eventually lead to failure, as previously mentioned [34]. Another factor that affects the service life of gas turbine hot components is the corrosive operating environment (high temperatures, low cyclic fatigue, fuel and air contamination, etc.). The physical GT model investigated in this study is made of stainless-steel grade 310. This material is prone to all previously mentioned phenomena due to its low heat conduction and high thermal expansion [35]. The GT and its CAD model are presented in Fig. 3

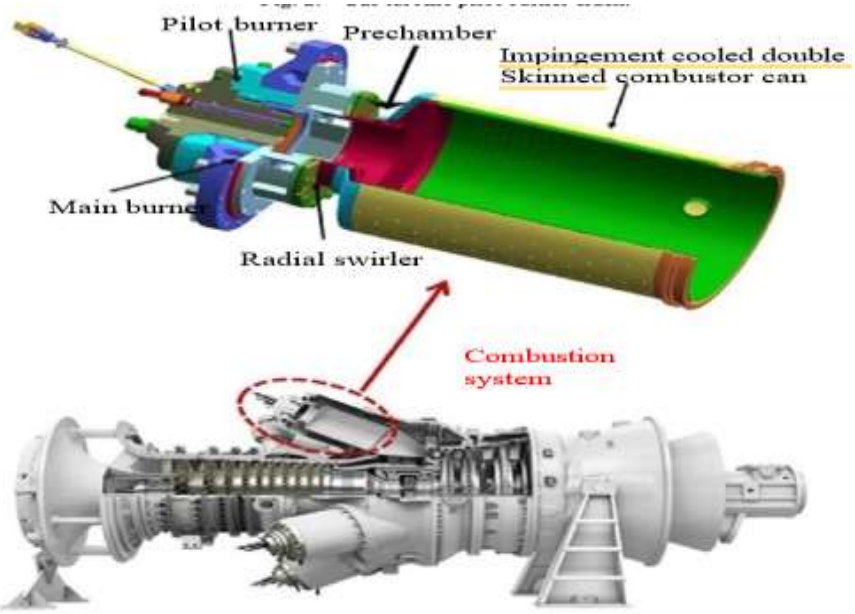

Figure 3: GT burner from inside (below is the physical model and above the CAD model of its combustion system) [36].

Due to the nature of the investigated fatigue failure and the GT operation condition, checked at annual service intervals or when a certain component fails, there is limited data regarding crack propagation before fatigue failure. Therefore, since temperatures and stresses represent the main parameters that directly affect the optimum structural performance and, thus, reduce the life of the GT. The objective of the proposed repair is to achieve a minimum overhaul of 32k hours.

As already mentioned, two repair scenarios are proposed to reduce the risk of crack occurrence and thus extend the burner life of the GT. Both are based on machining the damaged face of the existing pilot burners and then printing Hastelloy X (nickel-based superalloy) on top of the Stainless Steel 310 surface using AM techniques. The only difference is that additional cooling is provided in the second scenario. To check the effectiveness of each scenario, mechanical properties testing and mechanical analysis are performed. The material's mechanical properties can be determined using tensile and creep tests. Consequently, the mechanical analysis evaluates the component's design by performing calculations to determine the stress peaks, temperature distributions, fatigue life cycles, etc. This is typically achieved by doing finite element analysis (FEA) [37, 38]. Concerning the AM process itself, the Laser Beam Powder Bed Fusion (LB-PBF) method is deployed to print the Hastelloy X sections. This technique uses fine powders for superior surface finishing and thus, it contributes to the production of high-precision components with excellent mechanical properties. The LB-PBF technology is promising as it has the ability to repair damaged parts by printing complex metals layer by layer [39]. Using the LB-PBF, which is usually followed by Hot Isostatic Pressing (HIP) post-treatment, is a well-established approach which is implemented to ensure crack-free metallurgical bonding in repaired components, including the gas turbine burners. The limitations of this approach lie in the resulting residual stress and potential porosity, both of which are reducing of mitigation strategies including heat treatments and process optimization [40]. More information about the LB-PBF technique and its application fields can be found in [41-43].

2.1. Finite Element Modeling Procedure and Assumptions

To ensure a rigorous evaluation of the proposed repair scenarios, a coupled thermo-mechanical finite element analysis (FEA) was conducted using ANSYS®. The numerical model was developed to simulate the thermal loading conditions experienced by the pilot burner under full-load operation and to predict the resulting stress distribution and fatigue life.

2.2. Thermal Analysis

A steady-state thermal analysis was first performed to determine the temperature distribution within the burner geometry. The governing heat conduction equation applied in the model is:

$$\nabla\cdot(k\nabla T)+Q=0$$

Where:

k is the thermal conductivity,

T is temperature, and

Q represents internal heat generation (assumed negligible).

Boundary conditions were applied based on measured operating data from the test facility:

- Combustion-side temperature profile (Table 3)
- Convective heat transfer coefficient distribution
- Air temperature: T_Air=450^∘ C
- Fuel temperature: T_Fuel=20^∘ C

Material thermal properties were defined as temperature-dependent to capture realistic high-temperature behavior.

2.3. Structural Analysis

The temperature field obtained from the thermal analysis was imported into a structural static analysis to evaluate thermally induced stresses.

Thermal strain was calculated according to:

$$\varepsilon_{thermal} = \alpha \Delta T$$

Where:

α is the coefficient of thermal expansion and

ΔT is the temperature variation.

Linear elastic material behavior was assumed for both Stainless Steel 310 and Hastelloy X under high-temperature operating conditions. Perfect metallurgical bonding between the substrate and printed material was assumed at the interface.

The von Mises stress criterion was used to evaluate equivalent stress distribution:

$$\sigma_{vm} = \sqrt{\frac{1}{2}[(\sigma_1 - \sigma_2)^2 + (\sigma_2 - \sigma_3)^2 + (\sigma_3 - \sigma_1)^2]}$$

2.4. Mesh and Numerical Settings

The geometry was discretized using 3D solid elements (higher-order tetrahedral elements). A refined mesh was applied near:

- The burner face center
- The igniter hole
- The material transition interface

A mesh convergence study was performed to ensure that further mesh refinement resulted in negligible variation in the maximum stress values (<2% variation). The final mesh consisted of approximately 220,000 elements, which provided a balance between computational efficiency and solution accuracy.

2.5. Fatigue Life Estimation

Thermal fatigue life was estimated using a stress-based fatigue approach. Regions exhibiting high thermal stress concentration were evaluated against material fatigue strength data available in literature.

Crack initiation was predicted at locations where stress amplitude exceeded material fatigue limits under cyclic thermal loading. While a full low-cycle fatigue model was not implemented, the approach provides a conservative estimate of life expectancy under thermal cycling conditions.

2.6. Modeling Assumptions and Limitations

The following assumptions were adopted:

- Steady-state thermal loading
- Linear elastic material behavior
- Perfect bonding between base and printed material
- No creep deformation included
- No material degradation over time considered

These assumptions allow a comparative evaluation between repair scenarios while maintaining computational efficiency.

Table 1. Tensile properties (min) of the metal alloys and stainless steel at different temperature values (in MPa).

Material (0,2% Proof strength)	Temperature in °C					
	100	200	250	300	400	500
Stainless Steel (SS310)	176	157	147	136	125	119
Haynes 230	295	280	270	260	240	225
Hastelloy X	251	218	203	190	173	167

3. RESULTS AND DISCUSSION

3.1. Selection of the 3D printing material

AM techniques are particularly well-suited for making nickel-based superalloys, which are difficult to machine and have complex shapes in their applications, such as gas turbines [44]. Hastelloy X (Hast-X) is a nickel-chromium-iron-molybdenum-based superalloy that is easy to weld and form. It has high resistance to oxidation and stress corrosion cracking and good strength at high-temperatures, making it an attractive material for many high-temperature applications [45, 46]. To demonstrate the effectiveness of Hastelloy X in repairing the GT, its tensile and creep properties are presented and compared to the main material of the GT (Stainless Steel) and to Haynes230, which is another nickel-based alloy. Haynes230 is a nickel-chromium-tungsten-molybdenum alloy that combines excellent high-temperature strength and thermal stability with outstanding resistance to oxidizing environments [47, 48]. A comparison of the tensile properties of these materials is presented

in Table 1. The mean creep rupture strength of the same materials after being held for 100000 hours at specified temperatures is depicted in Table 2. The results of Table 2 are represented graphically in Fig. 4. It can be concluded from the material properties that were presented in the tables that Hastelloy X has better tensile strength and creep life than stainless steel. The following subsections will examine its mechanical characteristics with the FEA.

Table 2: Mean creep rupture strength of the metal alloys and stainless steel at different temperature values (in MPa).

Material	Temperature in °C							
	600	650	700	750	800	850	900	950
Stainless Steel (SS310)	83	49	25	14	8			
Haynes 230	213	150	104	75	50	29	19	8
Hastelloy X	194	127	83	53	32	18	9	4

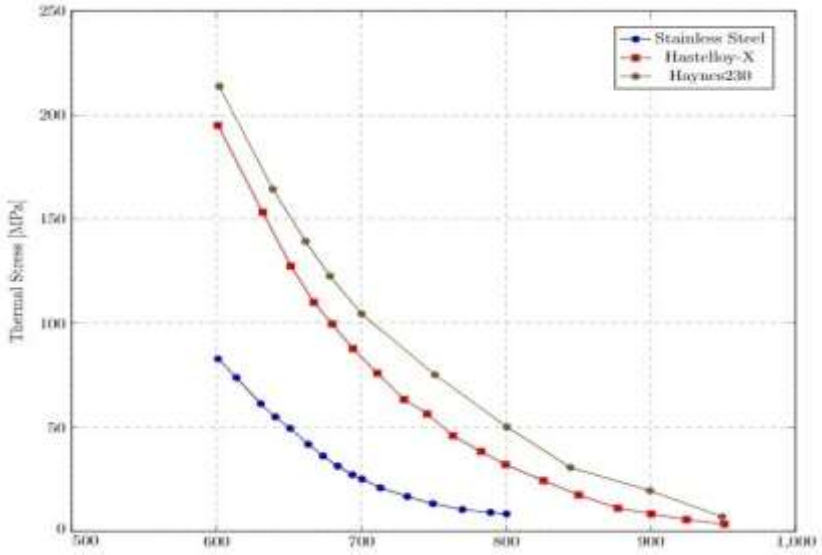

Figure 4: Mean creep fracture strength of stainless steel and metal alloys.

3.2. Scenario 1: 3D-Print of Hastelloy X on stainless steel top face without additional cooling

3.2.1. 3D print of 6 mm Hastelloy X

The objective was to remove 6 mm of the stainless-steel face of the pilot burner and replace it by printing 6 mm of Hastelloy X alloy. The partitioned CAD model of the pilot burner is presented in Fig. 5.

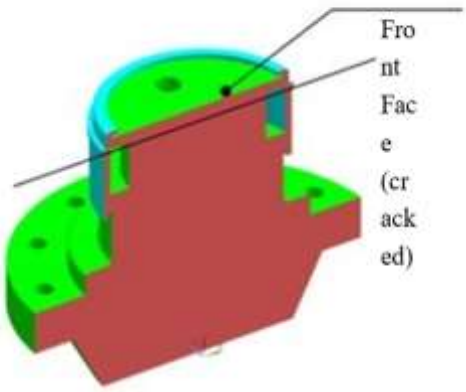

Figure 5: Front face of the GT pilot burner.

The FEA is conducted with the finite element package ANSYS®. An FEA model of the original GT with stainless steel only and an FEA model of the proposed repair with the 6 mm Hastelloy X layer will be created. The boundary conditions that are applied in the FEA models have been taken

from the test facility at full load. The air temperature was taken to be TAir = 450◦C, and the fuel temperature was taken to be TFuel = 20◦C. Moreover, the heat transfer coefficient and the temperatures at different locations from the centre face taken from the test facility were also used as boundary conditions for the FEA models. These values are presented in Table 3.

Table 3: FEA input temperature values at different locations from the pilot burner centre face

Description	**Temperature values at different locations**					
Point number	T14	T13	T12	T11	T10	T9
Distance from centre face [mm]	0	6	12	18	24	30
Temperature [˚C]	990	975	927	850	590	450

The contour plots of the heat transfer coefficient, and that of the temperature distribution are presented in Fig. 6.

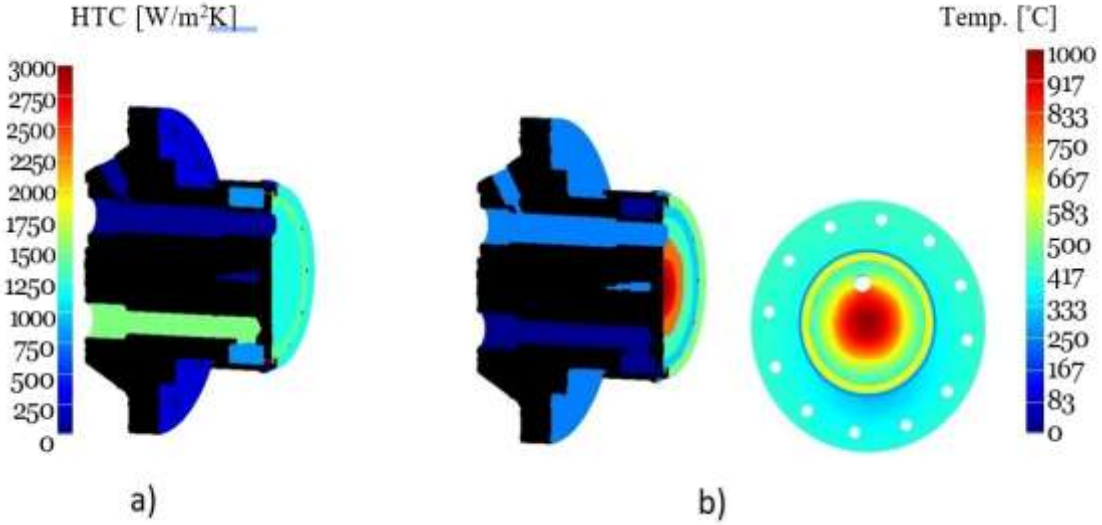

Figure 6: Contour plot of a) Heat transfer coefficient and b) Temperature distribution along the pilot burner

The idea is to create a realistic FEA model of the GT pilot burner with the same boundary conditions of the physical existing part and then to calculate the thermal stresses and life cycles for the existing burner with stainless steel and for the proposed repaired one with a 6 mm printed face of Hastelloy X. The thermal stresses that were induced in each of the FEA models are presented in Fig. 7.

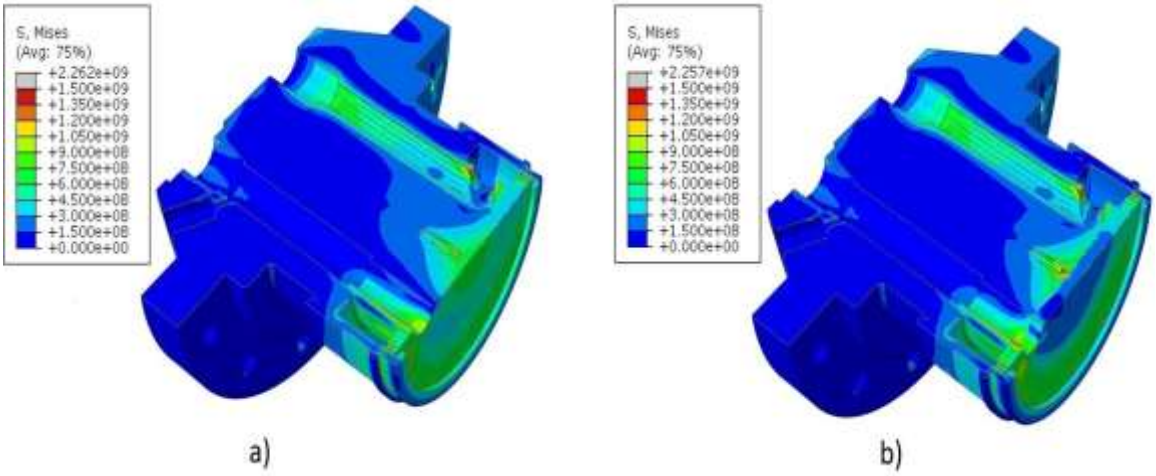

Figure 7: Contour plot of a) Stress distribution for stainless steel model and b) Stress distribution for model with 6 mm Hastelloy X

It can be noticed from the contour plot that the stress distribu- tion has decreased in the face centre with Hastelloy X, but increased at other locations, such as the igniter and thermocouple, in comparison to the stainless-steel model. Therefore, the depth of printed Hastelloy X should be increased from 6 mm to 50 mm (see the following subsection), where the operating temperature will be lower and the thermal expansion will be reduced. The thermal expansion coefficient of the stainless steel model was found to be 1.97e−05 at a temperature of 900◦C. As for the model with Hastelloy X, it was found to be 1.6e−05 at a temperature of 900◦C. This means there is about a 20% difference in the thermal expansion between stainless steel and the Hastelloy X. This high percentage in thermal expansion coefficient between the base and proposed materials will be one of the main causes of crack propagation as the high-stress locations appear between them. The life cycle has been investigated for the existing stainless steel material and the printed part with Hastelloy X face, as shown in Fig. 8.

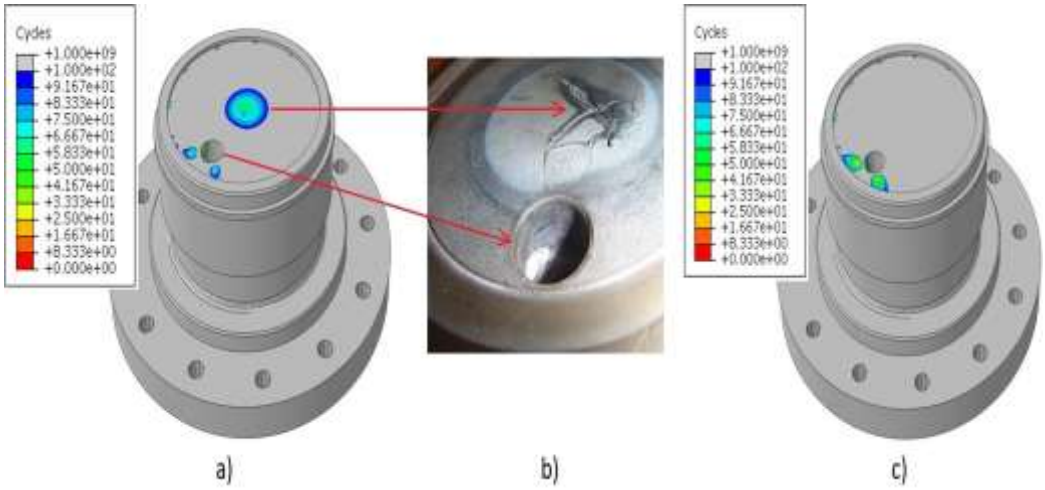

Figure 8: Contour plot of a) Life cycle for the stainless-steel model, b) The field observation of the physical stainless steel pilot burner face and c

Life cycle for the model with Hastelloy X face.

As for the stainless-steel model, the cracks have initiated at the face centre, the same location in the physical model from field observations. However, the face centre's life cycle with printed Hastelloy X face has improved. Nonetheless, this is not the case at the igniter hole, as Fig. 9 demonstrates. The crack initiation on the printed part has been observed on the layer between both materials. Furthermore, it happened at an early stage, approximately after 8 cycles. The FEA results show that the existing part would initially crack after approximately 8 cycles, which correlates to several observations from the operating field. As a result, Hastelloy X is acknowledged to be a better material to resist the high thermal stresses on this component, although a higher Hastelloy X thickness could reduce the remaining shortcomings that were addressed in this subsection.

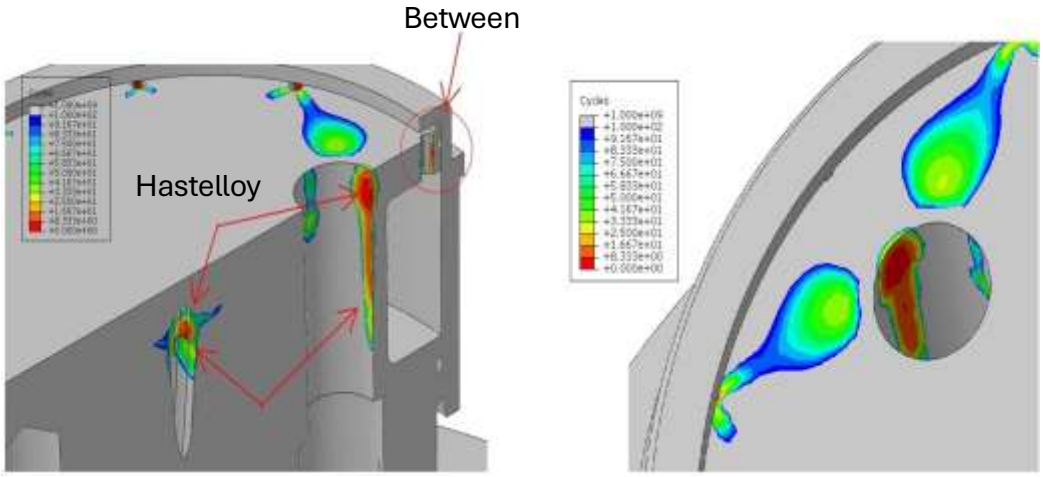

Figure 9: Contour plot of crack initiation at the igniter hole of the model with Hastelloy X face

3.2.2. 3D print of 50 mm Hastelloy X

To check the effect of the Hastelloy X thickness, 50 mm of the stainless-steel face of the pilot burner will be removed and then replaced by printing 50 mm of Hastelloy X alloy instead of 6 mm only as in the previous subsection. The interfaces, including igniter, thermocouple, etc. will stay the same as in the original design. During the printing process, a lightweight tree-like structure is produced to support the front face. This provides a lot of flexibility, and it reduces the stresses. The only drawback of this design is that the heat flux from the hot body to the cold body will also be reduced. The produced tree-like structure is presented in Fig. 10.

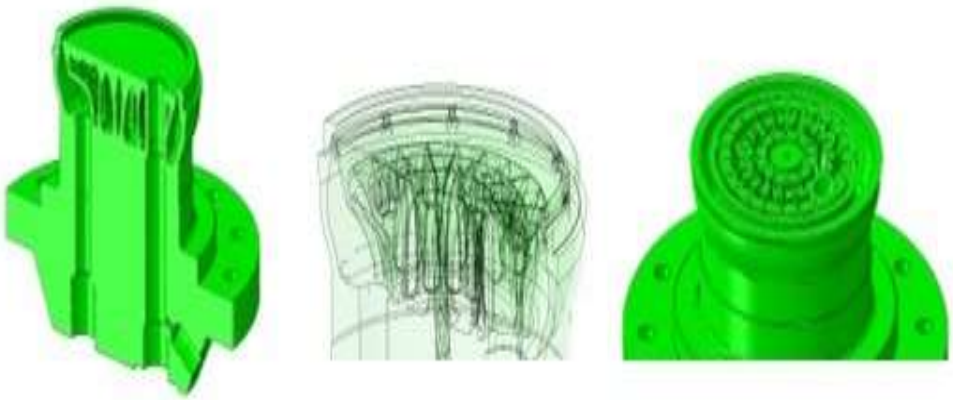

Figure 10: The tree-like structure of the GT pilot burner.

The results of the FEA are depicted in Fig. 11. The temperature at the face centre of the pilot burner was found to be 1254 ◦C. The stresses at the same location reached significantly high values, indicating severe thermal loading under this configuration. It can be concluded that Hastelloy X has a lower thermal expansion but a higher lifetime at elevated temperatures.

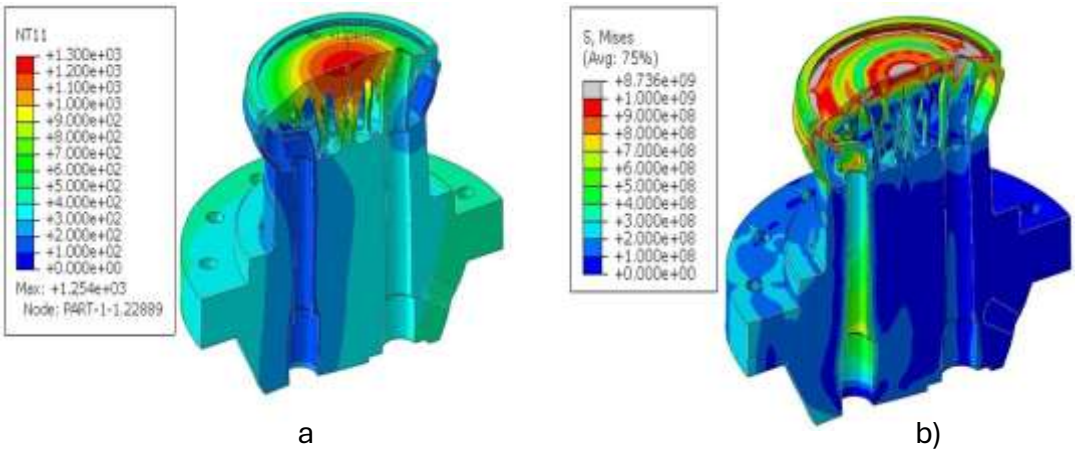

Figure 11: Contour plot of a) Temperature distribution and b) Stress distribution for model with 50 mm Hastelloy X.

Therefore, there will be reduced risk of cracks. Furthermore, the material transition will be moved to the low-temperature regions. Due to high temperatures, oxidation might still occur. Yet, the coating could still be added if needed to resolve this problem. As shown in Fig. 12a, the temperature increase on the cold side is too severe and negating the positive effect of increased stability. There will be a higher risk of material loss if a crack occurs.

3.2.3. Comparison of results between stainless steel, 6 mm and 50 mm Hastelloy X

As a result of the simulation, it can be concluded that the average stress at the hot surface of the burner for the case of 50 mm Hastelloy X is on the same level as in the original stainless-steel model. As Fig. 12 shows, the stress contour plots at the hot burner face look very similar between both models.

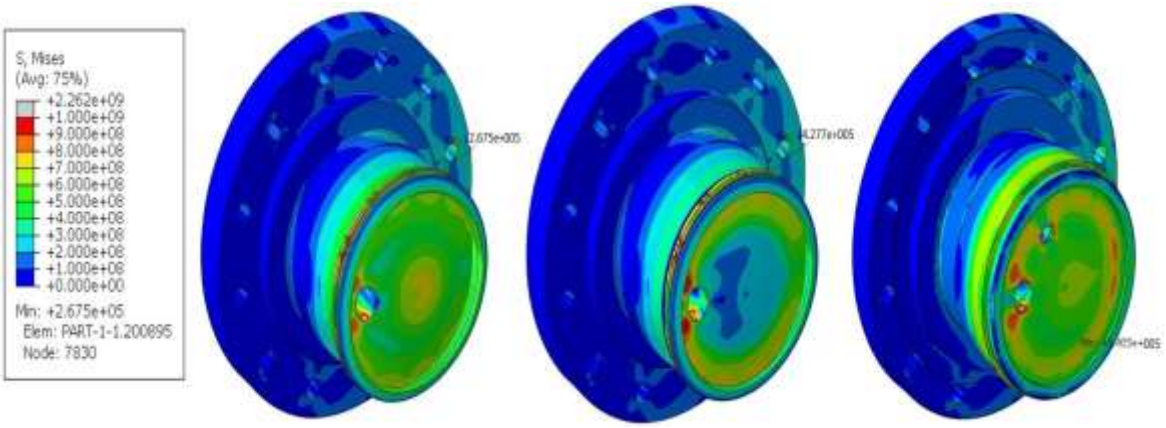

Figure 12: Stress contour at burner face of a) original model, b) repaired model with 6 mm Hastelloy X, and c) repaired model with

As previously mentioned, Hastelloy X has a lower thermal expansion value as stainless steel. It has also been observed that an additional tensile load is present in the model with a thin Hastelloy X layer due to the difference in thermal expansion. This is demonstrated in 50 mm Hastelloy X.

Fig. 13. The hot surface of the all-steel burner is in compression condition due to high temperature. If Hastelloy X layer is thin, the additional tensile load is present in it due to the difference in thermal expansion. The tensile load due to different expansion compensates for a part of compression stress due to high temperature - resulting in lower stress at the burner's front face. At the same time, at Hastelloy X steel transition, the stress is higher, and this causes additional critical locations. However, in the 50 mm Hastelloy X design, the effect of the additional tensile load is absent because the steel-Hastelloy X transition is in a low-temperature area. Therefore, the stress is back to its all-steel case level at the hot face.

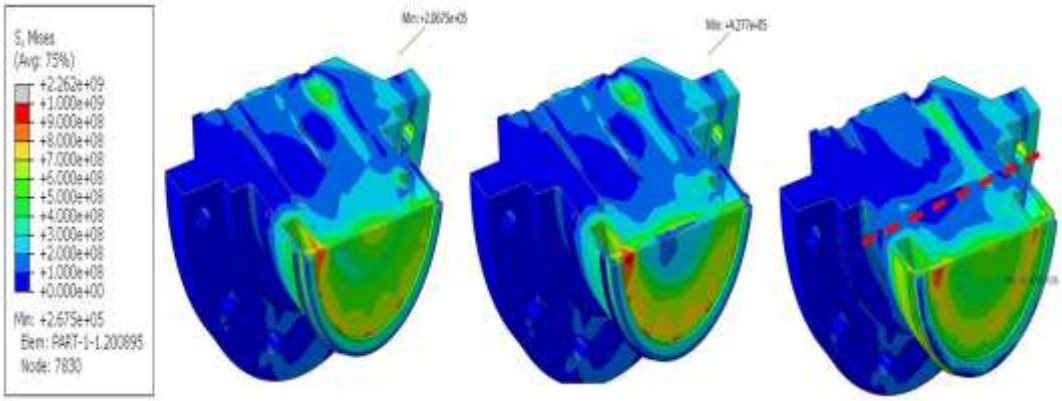

Figure 13: Stress contour at burner face section of a) original model, b) repaired model with 6 mm Hastelloy X, and c) repaired model with 50 mm Hastelloy X.

3.3. Scenario 2: 3D-Print of Hastelloy X on stainless steel top face with additional cooling

Since the first scenario proposed didn't deliver the expected results concerning a possible life extension of the GT burner by 32k hours of operation, this scenario still suggests using the first scenario with a 6 mm Hastelloy X thickness, yet together with imposed additional cooling. This is supposed to extend the GT burner life cycle. Therefore, a new FEA model with additional cooling holes was developed to achieve a better life cycle and lower repair costs. The proposed reverse engineering is presented in Fig. 14.

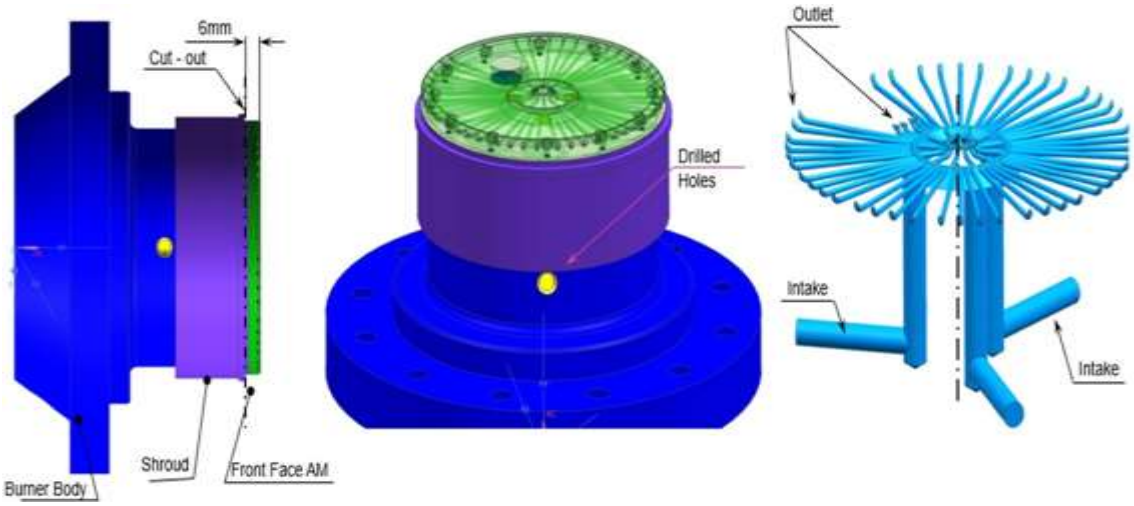

Figure 14: The CAD model of the pilot burner with additional cooling

As it can be seen in the figure, there are 3 intake holes, each with a diameter of 6 mm. There are 60 outlet channels, each with a diameter of 1.381 mm. The total volume of the printed components is approximately 3.49 ×10−5 m3. The amount of cooling air (50 g/s, as shown in Fig. 15) for the GT burner is taken from the rear stage of the GT compressor, and it has no impact on the total GT mass flow of 40 kg/s. Furthermore, the same boundary conditions applied in the FEA models used in the previous subsection were applied here. The air temperature was taken to be TAir = 450◦C, and the fuel temperature was taken to be TFuel = 20◦C. The same heat transfer coefficient and the temperatures at different locations from the centre face were taken from the test facility and used as boundary conditions for the FEA models. These values were already presented in Table 3.

It can be noted from Fig. 15 that the metal temperature has been decreased by approximately 225◦C compared to the original part without cooling (Fig. 6). In addition, the thermal expansion coefficient at 900◦C in Hastelloy X is 1.6e−5, and in stainless steel, is 1.57e−5, which shows good agreement. As a result, the life cycle expectation can be increased from 16k to 32k hours. A comparison of temperatures at the same location between the measured values at operating stainless steel GT, as well as simulations from the FEA models with a 6 mm thin Hastelloy X layer with- and without cooling, is depicted in Fig. 16. It is clear here that the temperature at the centre of the pilot burner face has been reduced by about 25% in the new proposed reverse engineering. The comparison between measured operating temperatures and simulated results demonstrates good agreement in trend and magnitude. The model successfully captures the thermal gradient from the burner center to the outer regions, confirming that the applied boundary conditions provide a realistic representation of operating conditions.

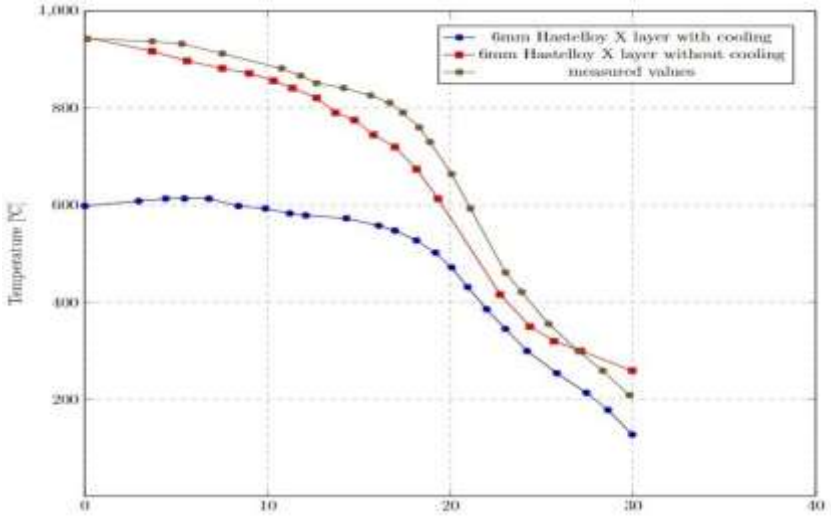

Figure 16: Results from the CAD model of the pilot burner with additional cooling.

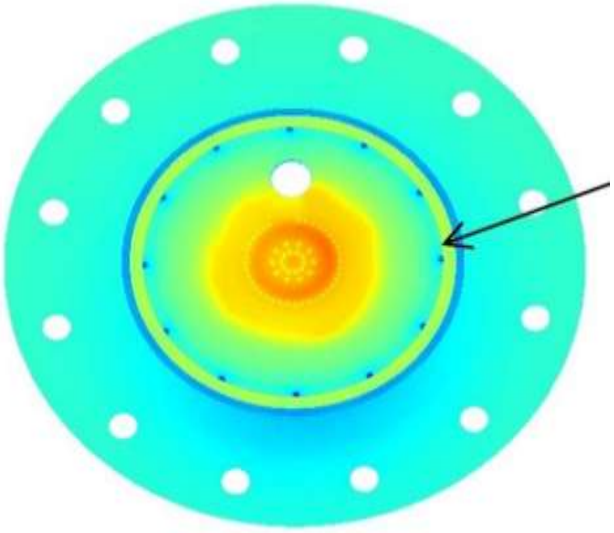

Temperature ~ 790◦C 50 g/s air used Lifetime: > 48 kh

Figure 15: The CAD model of the pilot burner with additional cooling

3.3.1. Comparative Summary of Repair Scenarios

To better illustrate the improvement achieved through additive manufacturing and additional cooling, a comparative summary of the investigated configurations is presented in Table 4.

Table 4: Comparative summary of repair scenarios

Configuration	Center Temperature (°C)	Observed Life Cycle	Key Observation
Stainless Steel (Original)	990	~8 cycles (field correlation)	Crack initiation at face center
6 mm Hastelloy X	Reduced locally	Limited improvement	Crack at material interface
6 mm Hastelloy X + Cooling	~790	32,000–48,000 h	Significant life extension

4. COST-SAVING ANALYSIS OF BURNER REPAIR WITH ADDITIVE MANUFACTURING

The study comprehensively analysed the cost savings associated with additive manufacturing (AM) burner repair compared to replacing new parts. Table 5 summarises the costs involved in both approaches. The cost of purchasing a new burner is $1, 329 per unit. In contrast, repairing a burner using AM techniques costs $872 per unit, with a repair yield of 97%. To give a better explanation of the cost savings, different repair scenarios were initially proposed: one with cooling and another without cooling. For the cost analysis, the outcome of one additional cycle (16, 000 hours) was considered, which represents Scenario 1 without cooling. The results demonstrate the potential cost savings achievable through the application of 3D printing repair. However, Scenario 2, which includes additional cooling, guarantees the achievement of two additional cycles (32, 000 hours) and presents the possibility of achieving up to three additional cycles (48, 000 hours). This illustrates the significant improvement in lifecycle and cost efficiency when combining 3D printing repair with enhanced cooling mechanisms. This demonstrates that AM repair is significantly less expensive than replacing the burner with a new part. The cost calculation also includes a correction factor or contingency risk to account for potential uncertainties and ensure the robustness of the financial analysis. This correction factor provides a more accurate and realistic assessment of the cost benefits. The findings indicate that substantial cost savings can be achieved through AM repair. Specifically, if each burner can successfully undergo three repair cycles, equating to 48, 000 operating hours, the total savings amount to approximately $1.22 million for repairing 450 burners. This significant reduction in costs highlights the economic viability of AM repair over purchasing new components. Additionally, enhanced cooling techniques make achieving the three-cycle lifespan with AM repair feasible. Improved cooling mechanisms can extend the operational life of the repaired burners, maximising the benefits of the AM repair process. This combination ensures the durability and performance of the repaired parts and further amplifies the cost-effectiveness by reducing the frequency of replacements.

It must be noted that in AM, the complexity factor is an adjustment to the repair or

manufacturing cost to account for the following aspects: Component Design Complexity, Material Challenges, Precision Requirements and Customization and Non-Standard Repairs. According to some studies from the literature, the complexity factor could reach about +40% [49, 50].

5. CONCLUSION

This study investigated pilot burners' failure mechanisms and proposed potential repair scenarios. A root cause analysis identified crack propagation and fractures as the key issues. Material selection was optimized for better thermal stress and thermal fatigue resistance. A comprehensive study, including the FEA of each proposed scenario, was conducted to assess the suitability of the repairs, and the results were compared to measured values.

The first scenario involved cutting the damaged stainless-steel layer of the pilot burner face to a thickness of 6 mm and replacing it with a 3D-printed Hastelloy X alloy of the same thickness. This initial approach was then iterated upon in the second scenario, where a 50 mm thickness (instead of 6 mm) of the damaged stainless steel was cut and replaced with the same 3D-printed Hastelloy X alloy thickness. However, the first scenario was deemed unsuitable due to the high difference in the thermal expansion coefficients between the base material and Hastelloy X, leading to crack initiation between the two materials.

The second scenario, a variant of the initial one but with additional cooling, showed significant promise. After conducting an FEA study and analyzing the repair cost versus the cost of a new

burner, it was concluded that the second scenario (printed Hastelloy X with additional cooling) holds the most potential for future development. This repair scenario could extend the pilot burn- ers' life cycle by 2 to 3 cycles, equivalent to 32, 000 to 48, 000 hours, due to the added cooling, thereby offering substantial operational benefits.

Currently, GT pilot burners have a lifespan of 16, 000 hours, which aligns differently from interim and major inspection schedules. To reduce maintenance costs, this project investigated repairing field-returned components with reverse engineering to extend their life to match the 32, 000 to 48, 000-hour cycle. It is concluded that a pilot burner repaired according to the second scenario has significant potential to achieve a service cycle of 32, 000 to 48, 000 operating hours, resulting in reduced workforce, unplanned downtime, and shutdown costs. Additionally, repairing a damaged pilot burner is less expensive than purchasing a new one.

Table 5: Cost saving analysis

Cost saving of burner repair with AM				
Turbines		Pilot Burner	Comments	Variables
Constraints	Costs of actual new burner	$1,329.80		
	Actual lifetime	16,000 h		
	AM costs repair (assumed)	$872.00	Estimation AM: from $621, Assumption: +40% complexity factor [55], [56]	$872.00
	Demand on burners / year	500		
	Yield rate of new repairs	97%	GT burner AM repair	97%
	Quantity of repaired burners	450	Formula: Demand × Yield rate	
Financial Impact			**Summary**	
	ONE ADDITIONAL CYCLE			
	Cost advantage for one cycle (16,000 h)	$206, 010.00	$206, 010.00	
	Correction factor (contingency risk)	$164, 808.00	**$164, 808.00**	20 %
	TWO ADDITIONAL CYCLES			
	Cost advantage for two cycles (32,000 h)	$804, 420.00	$804, 420.00	
	Correction factor (contingency risk)	$643, 536.00	**$643, 536.00**	20 %
	THREE ADDITIONAL CYCLES			
	Cost advantage for three cycles (48,000 h)	$1, 402, 830.00	$1, 402, 830.00	
	Correction factor (contingency risk)	$1, 122, 264.00	**$1, 122, 264.00**	20 %

FUTURE WORK

While experimental validation of the FEA results was beyond the scope of the present study, it

represents an important next step toward industrial implementation. Future work will include tensile, creep, and thermal fatigue testing of repaired burner samples to validate the numerical predictions. In addition, full-scale testing of repaired burners under simulated operating conditions is proposed to assess mechanical performance, thermal resistance, and long-term durability. These investigations will further strengthen the reliability and practical applicability of the proposed additive manufacturing repair strategy.

Acknowledgement: None

Conflict of Interest: The authors declare no conflict of interest.

Funding: The authors did not receive any external funding.

Data Availability: All of the data is present within the manuscript.

Author Contribution: Aiyad Gannan, first author:

Writing the whole paper. CFD analysis. Results discussion. Methodology.

Dr Wisam, abstract and approve reading. Result discussion

Dr Nader: writing literature. Methodology. Conclusion and reference. Result discussion.

Generative AI Declaration: This manuscript did not use any AI-assisted or generative AI technology.

REFERENCES

[1] Gade S, Vagge S, Rathod M. A review on additive manufacturing–methods, materials, and its associated failures. Advances in Science and Technology Research Journal. 2023;17(3).

[2] Jin B, Wang Q, Zhao L, Pan A, Ding X, Gao W, et al. A review of additive manufacturing techniques and post-processing for high-temperature titanium alloys. Metals. 2023;13(8):1327.

[3] Armstrong M, Mehrabi H, Naveed N. An overview of modern metal additive manufacturing technology. Journal of Manufacturing Processes. 2022;84:1001–29.

[4] Rajaguru K, Karthikeyan T, Vijayan V. Additive manufacturing–State of art. Materials today: proceedings. 2020;21:628–33.

[5] Srivastava M, Rathee S, Patel V, Kumar A, Koppad PG. A review of various materials for additive manufacturing: Recent trends and processing issues. Journal of Materials Research and Technology. 2022;21:2612–41.

[6] Tofail SA, Koumoulos EP, Bandyopadhyay A, Bose S, O'Donoghue L, Charitidis C. Additive manufacturing: scientific and technological challenges, market uptake and opportunities. Materials today. 2018;21(1):22–37.

[7] Mhetre G, Jadhav V, deshmukh S, Thakar C. A Review on Additive Manufacturing Technology. ECS Transactions. 2022;107:15355–74.

[8] Lettori J, Raffaeli R, Peruzzini M, Schmidt J, Pellicciari M. Additive manufacturing adoption in product design: An overview from literature and industry. Procedia Manufacturing. 2020;51:655–62.

[9] Huang Y, Leu MC, Mazumder J, Donmez A. Additive manufacturing: current state, future potential, gaps and needs, and recommendations. Journal of Manufacturing Science and Engineering. 2015;137(1):014001.

[10] Tao Y, Yin Q, Li P. An additive manufacturing method using large-scale wood inspired by laminated object manufacturing and plywood technology. Polymers. 2020;13(1):144.

[11] Williams A. Architectural modelling as a form of research. Arq: Architectural Research Quarterly. 2002;6(4):337–47.

[12] Taylor AD, Kim EY, Humes VP, Kizuka J, Thompson LT. Inkjet printing of carbon supported platinum 3-D catalyst layers for use in fuel cells. Journal of Power Sources. 2007;171(1):101–6.

[13] Lindwall A, Dordlofva C, Öhrwall Rönnbäck A, editors. Additive manufacturing and the product development process: Insights from the space industry. DS 87-5 Proceedings of the 21st International Conference on Engineering Design (ICED 17) Vol 5: Design for X, Design to X, Vancouver, Canada, 21-2508 2017; 2017.

[14] James WJ, Slabbekoorn MA, Edgin WA, Hardin CK. Correction of congenital malar hypoplasia using stereolithography for presurgical planning. Journal of oral and maxillofacial surgery. 1998;56(4):512–7.

[15] Tom T, Sreenilayam SP, Brabazon D, Jose JP, Joseph B, Madanan K, et al. Additive manufacturing in the biomedical field-recent research developments. Results in Engineering. 2022;16:100661.

[16] Wakjira Y, Akessa A, Lemu H. Overview study on challenges of additive manufacturing for a healthcare application. IOP Conference Series: Materials Science and Engineering. 2021;1201:012041.
[17] Wohlers T. Making products by using additive manufacturing. Manufacturing Engineering. 2011;146(4).
[18] Mohd Ghazali MI, Baharuddin AS, Alauddin MS, Dahlan A, Mohd. Fuzi SFZ, Shaarani SM, et al. Additive manufacturing food: technology and materials. Food Research. 2023;6:28–34.
[19] Gu S, Choi M, Park H, Jeong S, Doh J, Park S-i. Application of artificial intelligence in additive manufacturing. JMST Advances. 2023;5(4):93–104.
[20] Ciccone F, Bacciaglia A, Ceruti A. Optimization with artificial intelligence in additive manufacturing: a systematic review. Journal of the Brazilian Society of Mechanical Sciences and Engineering. 2023;45(6):303.
[21] Arjakine N, Bruck J, Grüger B, Seeger D, Wilkenhoener R. Advanced Weld Repair of Gas Turbine Hot Section Components2008.
[22] Jannesari Ladani L. Applications of artificial intelligence and machine learning in metal additive manufacturing. Journal of Physics: Materials. 2021;4(4):042009.
[23] Charles AP, Gonzalez Taylor CA. Development of a method to repair gas turbine blades using electron beam melting additive manufacturing technology. 2017.
[24] Wilson JM, Piya C, Shin YC, Zhao F, Ramani K. Remanufacturing of turbine blades by laser direct deposition with its energy and environmental impact analysis. Journal of Cleaner Production. 2014;80:170–8.
[25] Polyanskii S, Butakov S, Olkov I, Aleksandrov V. Repair of turbine components by abrasive-jet machining. Journal of Machinery Manufacture and Reliability. 2021;50(1):72–8.
[26] Schurb J, Hoebel M, Haehnle H, Kissel H, Bogdanic L, Etter T, editors. Additive manufacturing of hot gas path parts and engine validation in a heavy duty GT. Turbo Expo: Power for Land, Sea, and Air; 2016: American Society of Mechanical Engineers.
[27] Petrat T, Graf B, Gumenyuk A, Rethmeier M. Laser metal deposition as repair technology for a gas turbine burner made of inconel 718. Physics Procedia. 2016;83:761–8.
[28] Boyce MP. Gas turbine engineering handbook: Elsevier; 2011.
[29] Budynas RG, Nisbett JK. Shigley's mechanical engineering design: McGraw-Hill New York; 2008.
[30] Puspitasari P, Andoko A, Kurniawan P, editors. Failure analysis of a gas turbine blade: A review. IOP Conference series: materials science and engineering; 2021: IOP Publishing.
[31] Poursaeidi E, Kavandi A, Vaezi K, Kalbasi M, Arhani MM. Fatigue crack growth prediction in a gas turbine casing. Engineering Failure Analysis. 2014;44:371–81.
[32] Mazur Z, Pe´ rez-Herna´ ndez E, Garcia-Illescas R, editors. Gas Turbine Nozzle Life Assesment due to Thermal Fatigue. Turbo Expo: Power for Land, Sea, and Air; 2011.
[33] kamouri Yousefabad E, Asadi S, Savadkouhi P, Sedaghat O, Bakhshi A. The effect of non-uniform combustion temperature profile on thermal fatigue cracking of an air-cooled gas turbine vane. Engineering Failure Analysis. 2019;105:766–80.
[34] Moon H, Kim KM, Jeon YH, Shin S, Park JS, Cho HH. Effect of thermal stress on creep lifetime for a gas turbine combustion liner. Engineering Failure Analysis. 2015;47:34–40.
[35] Shi L, Northwood D. The mechanical behavior of an AISI type 310 stainless steel. Acta metallurgica et materialia. 1995;43(2):453–60.
[36] Agbonzikilo FE, Owen I, Stewart J, Sadasivuni SK, Riley M, Sanderson V. Experimental and numerical investigation of fuel–air mixing in a radial swirler slot of a dry low emission gas turbine combustor. Journal of Engineering for Gas Turbines and Power. 2016;138(6):061502.
[37] Hunter I, Daleo J, Wilson J, Ellison K. Analysis Of Hot Section Failures On Gas Turbines In Process Plant Service. 1999.
[38] Khan SU, Jamshed W. Finite element analysis and wear rate analysis of nano coated high speed steel tools for industrial application. Babylonian Journal of Mechanical Engineering. 2023;2023:12–9.
[39] Yuasa K, Tagami M, Yonehara M, Ikeshoji T-T, Takeshita K, Aoki H, et al. Influences of powder characteristics and recoating conditions on surface morphology of powder bed in metal additive manufacturing. The International Journal of Advanced Manufacturing Technology. 2021;115(11):3919–32.

[40] Abd-Elaziem W, Elkatatny S, Abd-Elaziem A-E, Khedr M, Abd El-baky MA, Hassan MA, et al. On the current research progress of metallic materials fabricated by laser powder bed fusion process: a review. Journal of Materials Research and Technology. 2022;20:681–707.
[41] Ji W, Zhou R, Viveganantha P, Wu MS, Gao H, Zhou K. Recent progress in gradient-structured metals and alloys. Progress in Materials Science. 2023;140:101194.
[42] Jamhari FI, Foudzi FM, Buhairi MA, Sulong AB, Radzuan NAM, Muhamad N, et al. Influence of heat treatment parameters on microstructure and mechanical performance of titanium alloy in LPBF: A brief review. Journal of Materials Research and Technology. 2023;24:4091–110.
[43] Alkhatib SE, Sercombe TB. High strain-rate response of additively manufactured light metal alloys. Materials & Design. 2022;217:110664.
[44] Dudzinski D, Devillez A, Moufki A, Larrouquère D, Zerrouki V, Vigneau J. A review of developments towards dry and high speed machining of Inconel 718 alloy. International journal of machine tools and manufacture. 2004;44(4):439–56.
[45] Hong H, Kim I, Choi B, Jeong H, Jo C. Effects of temperature and strain range on fatigue cracking behavior in Hastelloy X. Materials Letters. 2008;62(28):4351–3.
[46] Jinoop A, Paul C, Bindra K. Laser assisted direct energy deposition of Hastelloy-X. Optics & Laser Technology. 2019;109:14–9.
[47] Muhammad M, Ghiaasiaan R, Gradl PR, Shao S, Shamsaei N. Additively manufactured Haynes 230 by laser powder directed energy deposition (LP-DED): effect of heat treatment on microstructure and tensile properties. 2021.
[48] Schneider J, Williston D, Murphy T, Varner C, Hawkins J, Walker B. Solid state joining of nickel based alloy, Haynes 230. Journal of Materials Processing Technology. 2015;225:492–9.
[49] Bauer J, Malone P, editors. Cost estimating challenges in additive manufacturing. International Cost Estimating and Analysis Association Professional Development and Training Workshop; 2015.
[50] Thomas DS, Gilbert SW. Costs and cost effectiveness of additive manufacturing. NIST special publication. 2014;1176:12.